Effects of Dipole Moment, Linkers, and Chromophores at Side Chains on Long-Range Electron Transfer through Helical Peptides

Jun Watanabe, Tomoyuki Morita, and Shunsaku Kimura*

Department of Material Chemistry, Graduate School of Engineering, Kyoto University, Kyoto-Daigaku-Katsura, Nishikyo-ku, Kyoto 615-8510, Japan

Received: March 29, 2005; In Final Form: June 9, 2005

Octadecapeptides carrying a ferrocene moiety at the molecular terminal were self-assembled on gold, and long-range electron transfer from the ferrocene moiety to gold was investigated by electrochemical methods. Effects on electron transfer of dipole moment of helical peptides, linkers connecting the peptide to gold, and chromophores introduced into the side chains were discussed. Cyclic voltammetry of the monolayers in an aqueous solution revealed that long-range electron transfer over 40 Å occurred along the peptide molecule. Chronoamperometry showed that the long-range electron transfer should be ascribed to a hopping mechanism with use of amide groups as hopping sites. Electron transfer through the long peptide was not significantly accelerated by the dipole moment. However, the linker remarkably affected electron transfer depending on whether it was a methylene chain or a phenylene group, suggesting that local electron transfer between gold and the peptides should be the slowest step to determine the overall rate. Pyrenyl groups introduced into the side chains in the middle of the peptide molecule did not noticeably change electron transfer, probably because pyrenyl groups were too distant to allow direct electron transfer between them. Electrostatic potential profiles across the peptide monolayers were also calculated to explain reasonably the several interesting features in the present peptide systems.

Introduction

In biological systems, electron-transfer reactions efficiently occur along a sequential array of redox moieties surrounded by polypeptide matrixes.[1,2] These polypeptide matrixes are generally believed to act not only as scaffolds to fix the three-dimensional location of the redox moieties, but also as mediators to facilitate electron transfer. α-Helix is most frequently observed in such polypeptide matrixes and is considered to play an important role in the mediation of electron transfer.[3] The tunneling factor for electron transfer in a model α-helical peptide along its molecular axis has been reported to be 0.66 $Å^{-1}$, which is significantly smaller than that of alkyl chains, suggesting that helical peptides are a suitable medium for electron transfer.[4] Further, a large dipole moment along a helical peptide has been reported to remarkably accelerate electron transfer in the same direction due to the electric field.[5−8] Taken together, helical peptides are a good candidate for molecular wires especially with a rectifying property. Although the tunneling factor of helical peptides is larger than those of phenyleneethynylene[9,10] or phenylenevinylene[11,12] oligomers, which are intensively studied at the present moment as molecular wires, helical peptides have several advantages for the practical molecular electronic components in terms of well-specified molecular structure, facile molecular design of the molecular dimensions and arrangement of functional groups along the molecule, and a suitable self-assembling property to build up nanostructures, etc.

Electron transfer along helical peptides has been systematically studied by various groups. Generally, electron transfer between electron donor and acceptor under a large driving force generated by photoexcitation is well explained by a superexchange mechanism (electron tunneling). However, the superexchange mechanism will not be effective for long-range electron transfer because the rate of electron tunneling exponentially decays with an increase of the distance between donor and acceptor. From a practical point of view, such a strong distance dependency is unfavorable for molecular wires, because they are required to be equipped with the ability of long-range electron transfer.

One possible mechanism, which enables electron transfer over a long distance, is a hopping mechanism. Electrons are relayed with a moderate distance dependency by hopping the regularly arranged sites, which are electronically coupled to each other.[13,14] This mechanism has attracted growing attention in explaining the efficient long-range electron transfer in biological systems such as double strands of DNA.[15,16] It is therefore interesting to study helical peptide systems, where a hopping mechanism is operative, to clarify the ability of long-range electron transfer through helical peptides. In previous work, long-range electron transfer over 40 Å through helical hexadecapeptides, which were self-assembled on gold, was reported between a ferrocene moiety at the molecular terminal and gold under a small driving force.[17] The long-range electron transfer actually occurred through helical peptides, suggesting that a hopping mechanism should be operative by using regularly arranged amide groups as plausible hopping sites. In this work, we aimed to gain further understanding for long-range electron transfer through helical peptides. Effects on electron transfer of dipole moment, the linkers connecting the helical peptides and gold, and chromophores introduced into the side chains were studied.

Four kinds of long-chain helical octadecapeptides carrying a ferrocene moiety and a sulfur-containing group at the respective terminals were synthesized by the conventional liquid-phase

* Address correspondence to this author. E-mail: shun@scl.kyoto-u.ac.jp.

10.1021/jp051592g CCC: $30.25
Published on Web 07/08/2005

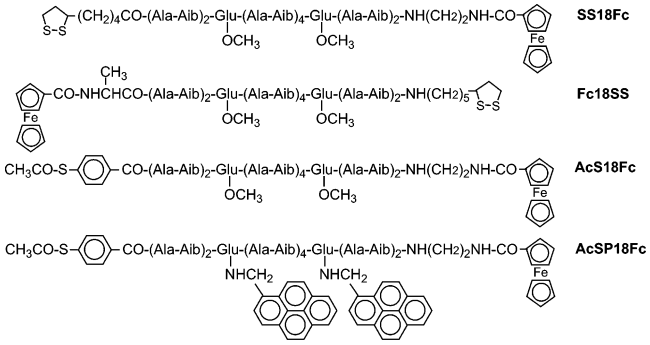

Figure 1. Chemical structures of the helical peptides. Ala, Aib, and Glu represent L-alanine, α-aminoisobutyric acid, and L-glutamic acid residues, respectively.

method (Figure 1). An alternating sequence of L-alanine and α-aminoisobutyric acid in the main chain is interrupted by insertion of L-glutamic acid derivatives at two positions. Two kinds of linkers, a disulfide group with a methylene chain and a thiophenyl group, are used to connect the helical peptides to gold. SS18Fc has a disulfide group at the N-terminal while Fc18SS has the same group at the C-terminal. Thus, when the respective peptides are immobilized on gold via a gold−sulfur linkage, they have a dipole moment opposite from each other. The other two peptides, AcS18Fc and AcSP18Fc, have an acetyl-capped thiophenyl group at the N-terminal and the latter has two pyrenyl groups at the side chains of the glutamic acid residues. The acetyl group was removed prior to self-assembling. Each peptide was self-assembled on gold by incubation of a gold substrate in the peptide solution, and the long-range electron transfer from the ferrocene moiety to gold was investigated by electrochemical methods. Comparisons of these helical peptide monolayers provide valuable information on long-range electron transfer through helical peptides.

Experimental Section

Synthesis of Helical Peptides. According to Scheme 1, SS18Fc, Fc18SS, AcS18Fc, and AcSP18Fc were synthesized from an octadecapeptide, Boc-(Ala-Aib)$_2$-Glu(OMe)-(Ala-Aib)$_4$-Glu(OMe)-(Ala-Aib)$_2$-OBzl (B18B), where Boc, Ala, Aib, Glu(OMe), and OBzl represent L-alanine, α-aminoisobutyric acid, L-glutamic acid methyl ester, and benzyl ester, respectively. This starting peptide was synthesized by the conventional liquid-phase method according to the literature.[18] Each final compound was obtained by coupling a ferrocene moiety and a sulfur-containing linker to the respective terminals after deprotection of the respective terminals. The ferrocene moieties (BC2Fc and FcAlaB) were designed so as to match the atom number between the sulfur atom and the ferrocene moiety in SS18Fc and Fc18SS. In the case of AcSP18Fc, two pyrenyl groups were introduced into the side chains of the two Glu residues via an amide linkage after hydrolysis of Glu(OMe) residues. All chemicals needed for the synthesis were purchased from commercial suppliers and used as received. All intermediates and final products were identified by ^{1}H NMR (400 MHz), and their purity was checked by thin-layer chromatography (TLC). A mixed solution of chloroform and methanol (5/1 v/v) was used for the TLC analysis. The final products were also confirmed by mass spectroscopy as well as NMR spectroscopy.

B18Fc. The benzyl group of B18B was deblocked by the catalytic hydrogenation in dichloromethane with 10 wt % of palladium carbon to afford B18OH. On the other hand, ferrocenecarboxylic acid (230 mg) was coupled with *tert*-butyloxycarbonylethylenediamine (160 mg) in chloroform with addition of *O*-(7-azabenzotriazol-1-yl)-1,1,3,3-tetramethyluronium hexafluorophosphate (HATU, 456 mg) and *N*,*N*-diisopropylethylamine (DIEA, 314 μL) at 0 °C for 2 h and thereafter at room temperature for 24 h. The solution was evaporated and the residue was washed with diisopropyl ether to afford BC2Fc (365 mg). BC2Fc was then treated with 4 N HCl in dioxane for 5 min to afford HC2Fc. B18OH (107 mg) and HC2Fc (100 mg) were coupled in chloroform with addition of HATU (37 mg) and DIEA (82 μL) under N_2 atmosphere at 0 °C for 2 h and thereafter at room temperature for 36 h. The solution was evaporated and the crude product was purified by a Sephadex LH20 column (methanol as eluant) to afford the product (76 mg, 61%). TLC: R_f 0.61. ^{1}H NMR (400 MHz, CD_3OD): δ (ppm) 1.3−1.6 (81H, $(CH_3)_3C$, AlaCβH_3, AibCβH_3), 2.1−2.3 (4H, GluCγH_2), 2.4−2.7 (4H, GluCβH_2), 3.4−3.6 (4H, NH-(CH_2)NH), 3.63 (6H, s, OCH_3), 3.8−4.3 (10H, AlaCαH, GluCαH), 4.2−5.0 (9H, ferrocenyl-*H*), 7.3−8.5 (20H, N*H*). MS (FAB, matrix; nitrobenzyl alcohol): *m*/*z* 1929.9 (calcd for $C_{86}H_{138}FeN_{20}NaO_{25}$ [(M + Na)$^+$] *m*/*z* 1929.94).

SS18Fc. B18Fc was treated with 4 N HCl in dioxane for 10 min to afford H18Fc. Lipoic acid (19 mg) was coupled to H18Fc (68 mg) in chloroform with the addition of HATU (17 mg) and DIEA (18 mL) under N_2 atmosphere at 0 °C for 2 h and thereafter at room temperature for 30 h. The solution was condensed and the crude product was purified by a Sephadex LH20 column (chloroform/methanol = 1/1 v/v as eluant) to afford the product (50 mg, 68%). TLC: R_f 0.55. ^{1}H NMR (400 MHz, CD_3OD): δ (ppm) 1.3−1.6 (78H, SSCH$_2$CH$_2$CH(CH_2)$_3$-CH_2CO, AlaCβH_3, AibCβH_3), 1.86, 2.42 (2H, m, SSCH$_2$CH_2-CH(CH_2)$_3$CH$_2$CO), 2.1−2.3 (4H, GluCγH_2), 2.35 (2H, m, SSCH$_2$CH$_2$CH(CH_2)$_3$CH_2CO), 2.4−2.7 (4H, GluCβH_2), 3.13 (2H, m, SSCH_2CH$_2$CH(CH_2)$_3$CH$_2$CO), 3.4−3.6 (5H, NH-(CH_2)NH, SSCH$_2$CH$_2$C*H*(CH_2)$_3$CH$_2$CO), 3.63, 3.64 (6H, s, OCH_3), 3.8−4.3 (10H, AlaCαH, GluCαH), 4.2−5.0 (9H, ferrocenyl-*H*), 7.4−8.5 (20H, N*H*). MS (FAB, matrix; nitrobenzyl alcohol): *m*/*z* 2018.0 (calcd for $C_{89}H_{142}FeN_{20}NaO_{24}S_2$ [(M + Na)$^+$] *m*/*z* 2017.92).

B18SS. Ferrocenecarboxylic acid (115 mg) was coupled with L-alanine benzyl ester *p*-tosylate (176 mg) in chloroform with the addition of HATU (228 mg) and DIEA (244 μL) at 0 °C for 2 h and thereafter at room temperature for 18 h. The solution was evaporated and the crude product was purified by a Sephadex LH20 column (methanol as eluant) to afford FcAlaB (161 mg). The benzyl group of FcAlaB was then deblocked by catalytic hydrogenation in dichloromethane with 10 wt % of palladium carbon to afford FcAlaOH. On the other hand, B18OH (50 mg) was reacted with 1,2-dithia-3-(1-amino-*n*-pentyl)cyclohexane hydrochloride[7] (17 mg) in chloroform with the addition of HATU (14 mg) and DIEA (23 μL) at 0 °C for 2 h and thereafter at room temperature for 48 h. The solution was evaporated and the crude product was purified by a Sephadex LH20 column (methanol as eluant) to afford B18SS (55 mg). The Boc group of B18SS was then removed with 4 N HCl in dioxane for 20 min to afford H18SS. FcAlaOH (45 mg) and H18SS (53 mg) were coupled in chloroform with the addition of HATU (17 mg) and DIEA (17 μL) under N_2 atmosphere at 0 °C for 2 h and thereafter at room temperature for 45 h. The solution was evaporated and the crude product was purified by a Sephadex LH20 column (chloroform/methanol = 1/1 v/v as eluant) to afford the product (44 mg, 73%). TLC: R_f 0.50. ^{1}H NMR (400 MHz, CD_3OD): δ (ppm) 1.3−1.6 (80H, AlaCβH_3, AibCβH_3, NHCH$_2$(CH_2)$_4$CHCH$_2$CH$_2$SS), 1.86, 2.42 (2H, m, NHCH$_2$(CH_2)$_4$CHCH_2CH$_2$SS), 2.1−2.3 (4H, GluCγH_2),

SCHEME 1: Synthetic Scheme of the Helical Peptides

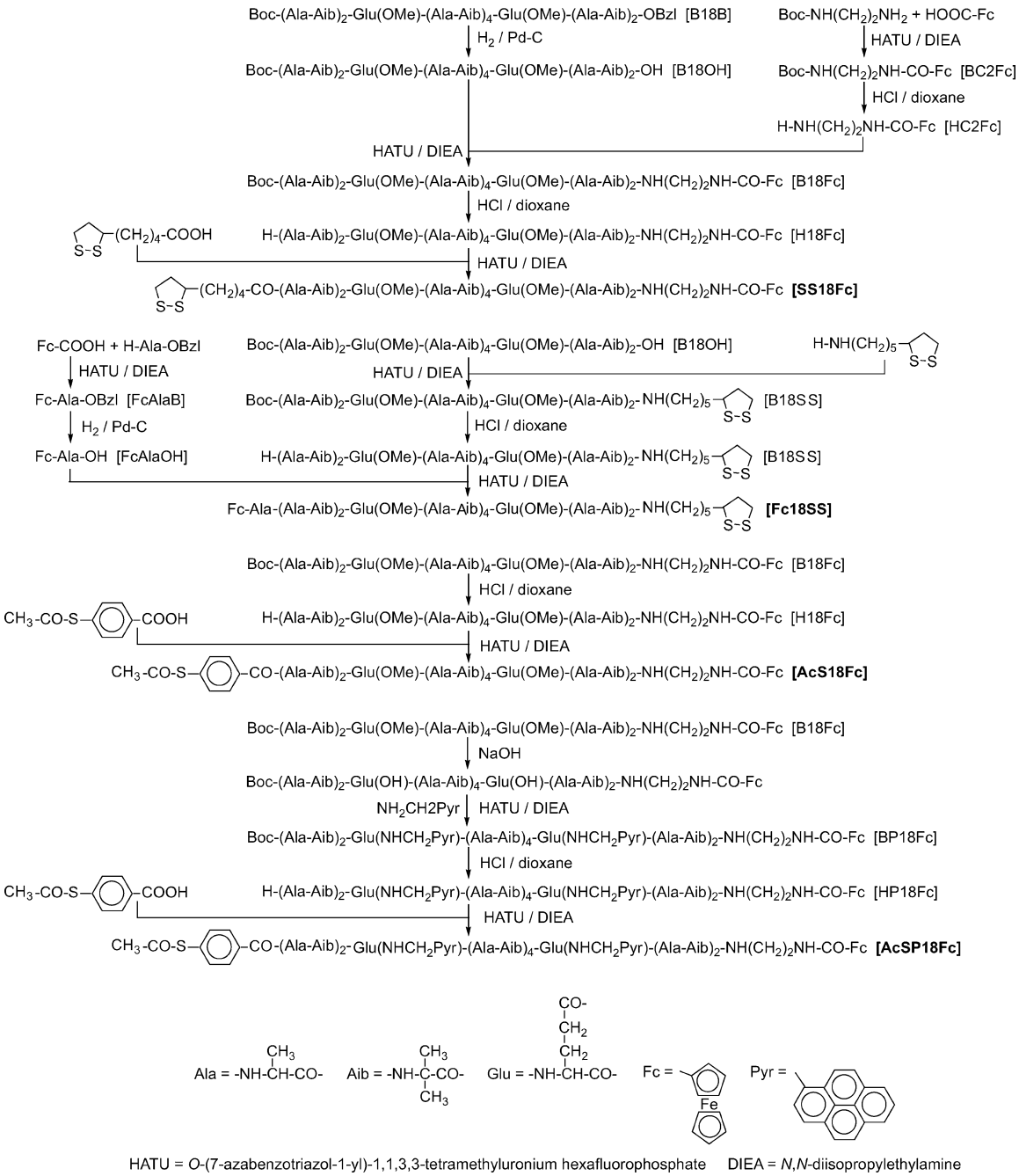

2.4−2.7 (4H, GluCβH_2), 3.00, 3.35 (2H, br m, NHCH_2(CH$_2$)$_4$-CHCH$_2$CH$_2$SS), 3.40 (2H, m, NHCH$_2$(CH$_2$)$_4$CHCH$_2$CH_2SS), 3.52 (1H, m, NHCH$_2$(CH$_2$)$_4$CHCH$_2$CH$_2$SS), 3.62, 3.64 (6H, s, OCH_3), 3.8−4.3 (11H, AlaCαH, GluCαH), 4.2−5.0 (9H, ferrocenyl-*H*), 7.4−8.2 (20H, N*H*). MS (FAB, matrix; nitrobenzyl alcohol): *m*/*z* 2031.9 (calcd for $C_{90}H_{144}FeN_{20}NaO_{24}S_2$ [(M + Na)$^+$] *m*/*z* 2031.94).

AcS18Fc. B18Fc was treated with 4 N HCl in dioxane for 10 min to afford H18Fc. Acetyl chloride was reacted to 4-thiobenzoic acid to yield 4-(*S*-thioacetyl)benzoic acid. The synthesized 4-(*S*-thioacetyl)benzoic acid (51 mg) was coupled to H18Fc (96 mg) in chloroform with the addition of HATU (30 mg) and DIEA (30 mL) under N_2 atmosphere at 0 °C for 2 h and thereafter at room temperature for 24 h. The solution was removed and the crude product was purified by a Sephadex LH20 column (chloroform/methanol = 1/1 v/v as eluant) to afford the product (68 mg, 65%). TLC: R_f 0.52. ^{1}H NMR (400 MHz, CD_3OD): δ (ppm) 1.3−1.6 (72H, AlaCβH_3, AibCβH_3), 2.1−2.3 (4H, GluCγH_2), 2.41 (3H, s, CH_3COS), 2.4−2.7 (4H, GluCβH_2), 3.4−3.6 (4H, NH(CH_2)NH), 3.59 (6H, s, OCH_3), 3.8−4.3 (10H, AlaCαH, GluCαH), 4.2−5.0 (9H, ferrocenyl-*H*), 7.2−8.4 (24H, N*H*, phenylene-*H*). MS (FAB, matrix; nitrobenzyl alcohol): *m*/*z* 2007.9 (calcd for $C_{90}H_{136}FeN_{20}NaO_{25}S$ [(M + Na)$^+$] *m*/*z* 2007.90).

AcSP18Fc. B18Fc (19 mg) was dissolved in a mixed solvent of methanol and dioxane (1/1 v/v) and a 1 N NaOH aqueous solution (2.3 μL) was added to the reaction solution dropwise. After the mixture was stirred for 4 h, chloroform was added to

the reaction solution and the solution was washed successively with a 4 wt % $KHSO_4$ aqueous solution and a saturated NaCl aqueous solution. The organic phase was dried over $MgSO_4$. The solution was concentrated, and the residue was washed with diisopropyl ether to afford a solid (20 mg). This solid was then reacted with 1-pyrenemethylamine hydrochloride (27 mg) in chloroform with the addition of HATU (5.7 mg) and DIEA (21 μL) under N_2 atmosphere at 0 °C for 2 h and thereafter at room temperature for 48 h. The solution was removed and the crude product was purified by a Sephadex LH20 column (methanol) to afford BP18Fc (11 mg). The Boc group of BP18Fc was removed with 4 N HCl in dioxane for 10 min to afford HP18Fc. 4-(*S*-thioacetyl)benzoic acid (4.4 mg) was coupled to HP18Fc in chloroform with the addition of HATU (2.6 mg) and DIEA (2.5 μL) under N_2 atmosphere at 0 °C for 2 h and thereafter at room temperature for 36 h. The solution was removed and the crude product was purified by a Sephadex LH20 column (methanol as eluant) to afford the product (6.0 mg, 25%). TLC: R_f 0.57. ^{1}H NMR (400 MHz, CD_3OD): δ (ppm) 1.3−1.6 (72H, AlaCβH_3, AibCβH_3), 2.1−2.3 (4H, GluCγH_2), 2.40 (3H, s, CH_3COS), 2.4−2.7 (4H, GluCβH_2), 3.4−3.6 (4H, NH-(CH_2)NH), 3.8−4.2 (10H, AlaCαH, GluCαH), 4.2−5.0 (9H, ferrocenyl-*H*), 5.09 (4H, dd, pyrenyl-CH_2), 7.2−8.4 (42H, N*H*, phenylene-*H*, pyrenyl-*H*). MS (FAB, matrix; nitrobenzyl alcohol): *m*/*z* 2407.0 (calcd for $C_{122}H_{154}FeN_{22}NaO_{23}S$ [$(M + Na)^+$] *m*/*z* 2406.05).

Circular Dichroism (CD) Spectroscopy. CD spectra of the peptides were measured in ethanol on a CD spectropolarimeter (J-600, JASCO Co., Ltd., Japan). The measurement was carried out with an optical cell of 0.1 cm optical path length at 20 °C. The residue concentration was set to be 4.0×10^{-4} M. The helix content of the peptide was calculated from the following formula,[19] $f_H = -([\theta]_{222} + 2340)/30300$, in which f_H and $[\theta]_{222}$ represent the helix content and molar ellipticity in concentration of residue at 222 nm.

Absorption and Fluorescence Spectroscopy. The absorption spectrum of AcSP18Fc in ethanol was recorded at the concentration of 1.0×10^{-5} M on a Ubest-50 spectrometer (Jasco Co., Ltd., Japan). The fluorescence spectrum in ethanol was recorded at the concentration of 1.0×10^{-6} M on an F-4010 fluorometer (Hitachi Co., Ltd., Japan). Each measurement was carried out at room temperature.

Preparation of Self-Assembled Monolayers. A slide glass was washed thoroughly with methanol and distilled water followed by sulfonic acid for 3 h. A substrate coated with gold was prepared by vapor deposition of chromium and then gold (99.99%) onto the slide glass. The thickness of the chromium and gold layers, monitored by a quartz oscillator, were approximately 500 and 2000 Å, respectively. The prepared gold substrate was immediately used for self-assembling. The gold substrate was incubated in an ethanol solution of the helical peptide (0.1 mM) for 24 h. After incubation, the substrate was rinsed rigorously with ethanol and dried in a steam of dry N_2 and in vacuo for 15 min. The capping acetyl group of AcS18Fc or AcSP18Fc was removed by treatment with 10 μL of 28 wt % ammonia water for 10 min prior to self-assembling.

Fourier Transform Infrared Reflection-Absorption Spectroscopy (FTIR-RAS). The FTIR spectra were recorded on a Fourier transform infrared spectrometer (Magna 850, Nicolet Japan Co., Ltd., Japan) at room temperature. For RAS measurements, a reflection attachment (model RMA-1DG/VRA, Harrick Co,. Ltd., NY) was used. The incident angle was set at 85° from the surface normal. The number of interferogram accumulations was 1000. Molecular orientation of the peptide monolayer on the gold substrate was determined on the basis of the amide I/amide II absorbance ratio in the FTIR-RAS spectrum according to eq 1 under the assumption of a uniform orientation of the helix axis around the surface normal.[20]

$$I_1/I_2 = 1.5((3\cos^2\gamma - 1)(3\cos^2\theta_1 - 1) + 2)/((3\cos^2\gamma - 1)(3\cos^2\theta_2 - 1) + 2) \quad (1)$$

I_i, γ, and θ_i ($i = 1$ or 2 corresponding to amide I or amide II) represent the observed absorbance, the tilt angle of helical axis from the surface normal, and the angle between the transition moment and the helix axis, respectively. The values of θ_1 and θ_2 are taken to be 39° and 75°, respectively.[21,22]

Electrochemical Studies (cyclic voltammetry and chronoamperometry). Electrochemical experiments were performed in a three-electrode system with the gold substrate as the working electrode, Ag/AgCl in 3 M NaCl as the reference electrode, and a platinum wire as the auxiliary electrode. The supporting electrolyte was a 1 M $HClO_4$ aqueous solution. The water for the solution was distilled and passed through a Milli-Q purification system. Cyclic voltammetry and chronoamperometry experiments were carried out with a voltammetric analyzer (model 604, BAS Co., Ltd., Japan) at room temperature. All solutions were deaerated by passing N_2 gas through them for 20 min prior to the measurements. All the applied potentials of the gold substrates reported in the results were measured with respect to the reference electrode. The area of the working electrode exposed to the electrolyte solution was 0.9−1.1 cm^2. The uncompensated resistance of the cell was estimated by ac voltammetry to be ca. 4 ohm. In the chronoamperometry, the time constant in the current follower of the potentiostat was set at 10^{-4} s. The potential was changed symmetrically with respect to the standard redox potential: in the case of a standard redox potential of 0.45 V and an overpotential of ±0.04 V, the potential was applied from 0.41 to 0.49 V for the ferrocene oxidation, and then returned back to 0.41 V for the ferricinium reduction.

Calculation of Molecular Orbital Energies. The energies of the orbitals localized on the ferrocene moiety, the sulfur atom, and the amide group were calculated by using model compounds, ferrocene, 1,2-dithiolane, and *N*-acetoamide, respectively, as follows. The initial geometry of each compound was generated by the CAChe software[24] (Fujitsu Co., Ltd., Japan), and was optimized by a semiempirical Austin Model 1 (AM1) method in the MOPAC 2002 package. Using the obtained geometry as input, ab initio calculation was carried out with use of the Gaussian 03 program.[25] The geometry was further optimized at the Hartree−Fock (HF) level. With the optimized geometry at the HF level, the single-point energy was calculated based on density functional theory with Becke's three-parameter hybrid functional and the Lee−Yang−Parr correlation (B3LYP) method to obtain the frontier orbital energies with respect to the vacuum level. The basis sets for ab initio calculation were the 6-31G(d) basis set for C, H, N, O, and S atoms and the Dunning/Huzinaga full double-ζ (LanL2DZ) basis set for the Fe atom, respectively.

Calculation of Electrostatic Potential Profiles through the Monolayer. Theoretical electrostatic potential profiles through the SS18Fc and Fc18SS SAMs on various applied potentials were calculated on the basis of the metal/organic/solution model.[26,27] In our case, the system is composed of six regions: gold, gold surface−sulfur atom, methylene linker, helical peptide, the connector between the peptide and the ferrocene moiety, and the aqueous phase. According to Gauss' law, the

electrostatic potentials at the metal (ϕ_1), the sulfur atom (ϕ_2), the peptide terminal near gold (ϕ_3), the other peptide terminal (ϕ_4), the ferrocene moiety (ϕ_5), and the aqueous phase (ϕ_6) are related to the individual charge densities (σ_1, σ_2, σ_3, σ_4, σ_5, and σ_6) as in eqs 2−7.

$$\sigma_1 = (\epsilon_0\epsilon_a)(\phi_1 - \phi_2)/d_a \quad (2)$$

$$\sigma_1 + \sigma_2 = (\epsilon_0\epsilon_b)(\phi_2 - \phi_3)/d_b \quad (3)$$

$$\sigma_1 + \sigma_2 + \sigma_3 = (\epsilon_0\epsilon_c)(\phi_3 - \phi_4)/d_c \quad (4)$$

$$\sigma_1 + \sigma_2 + \sigma_3 + \sigma_4 = (\epsilon_0\epsilon_d)(\phi_4 - \phi_5)/d_d \quad (5)$$

$$\sigma_6 = -(2\epsilon_0\epsilon_e\kappa kT/e)\sinh(e(\phi_5 - \phi_6)/2kT) \quad (6)$$

$$\sigma_1 + \sigma_2 + \sigma_3 + \sigma_4 + \sigma_5 + \sigma_6 = 0 \quad (7)$$

Equation 7 expresses charge neutrality. In these formulas, ϵ_0, e, k, and T have the usual meaning. The constant, κ, is the reciprocal of the Debye length (ca. 0.33 $Å^{-1}$ in a 1 M $HClO_4$ aqueous solution). The values ϵ_a, ϵ_b, ϵ_c, ϵ_d, and ϵ_e represent the relative dielectric constants of the respective layers, the gold surface−sulfur atom (a), the methylene linker (b), the helical peptide (c), and the connector between the peptide and the ferrocene moiety (d), and that in the aqueous phase (e). The d_a, d_b, d_c, and d_d values are the thicknesses of the respective layers. These values were set as follows: $\epsilon_a = 2.7$, $\epsilon_b = 2.3$,[28] $\epsilon_c = 3.0$,[27] $\epsilon_d = 2.3$,[28] $\epsilon_e = 78$, $d_a = 2$ Å,[28] $d_b = 4$ Å, $d_c = 23$ Å, and $d_d = 3$ Å, respectively. The ϵ_a value was obtained by correcting the reported value for alkanethiol self-assembled monolayer[28] (6.4) by the density of the sulfur atom on the surface in the present monolayer (0.015 Au−S/Å^2). As the exact thicknesses of the layers (b) and (d) are unknown, the half values of the length of a fully extended chain are assumed. The d_c value was calculated from the length of the helical peptide and tilt angle of 30°. Adsorption of organic molecules on the metal surface generally reduces the dipole moment that the metal originally has to vacuum (metal$^+$−vacuum$^-$).[30,31] This effect can be conveniently expressed by the formation of a dipole moment from the metal surface to the organic surface (metal$^-$−organic$^+$). In most cases of alkanethiol SAMs on gold, this dipole moment surpasses the opposite dipole moment caused by the ionic property of the gold−sulfur linkage (Au$^+$−S$^-$), generating ca. +500 mV potential drop.[28,32] In our case, the probable potential drop is calculated to be ca. 150 mV by correcting by the density of the sulfur atom on the surface. To express this potential drop, the charge density of the sulfur atom, σ_2, was set to be +0.02 C/m^2. The charge densities of the peptide terminals were taken to be ±0.004 C/m^2. By using these values, the experimental surface potentials of hexadecapeptide monolayers immobilized at the N- and C-terminals (−150 mV and +350 mV)[33] were successfully reproduced in the similar gold/monolayer/vacuum model. The σ_5 value is zero due to the neutral nature of this layer. The electrostatic potential of gold (ϕ_1) and the aqueous phase (ϕ_6) with respect to the potential of the reference Ag/AgCl electrode (ϕ_{ref}) can be obtained from eqs 8 and 9 by using the applied potential (E_{app}) and the potential at zero charge (E_{pzc}), respectively.

$$\phi_1 = \phi_{ref} + E_{app} \quad (8)$$

$$\phi_6 = \phi_{ref} + E_{pzc} \quad (9)$$

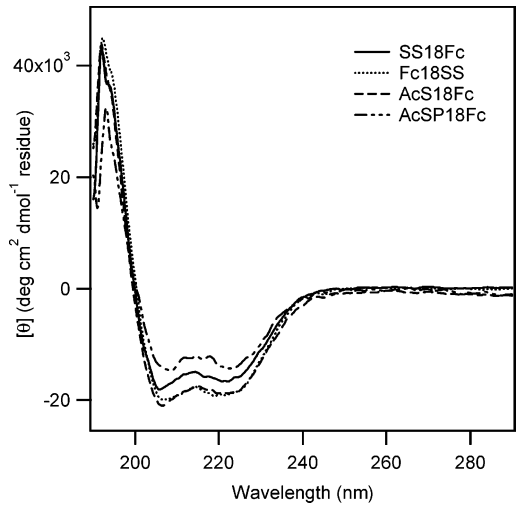

Figure 2. CD spectra of the peptides.

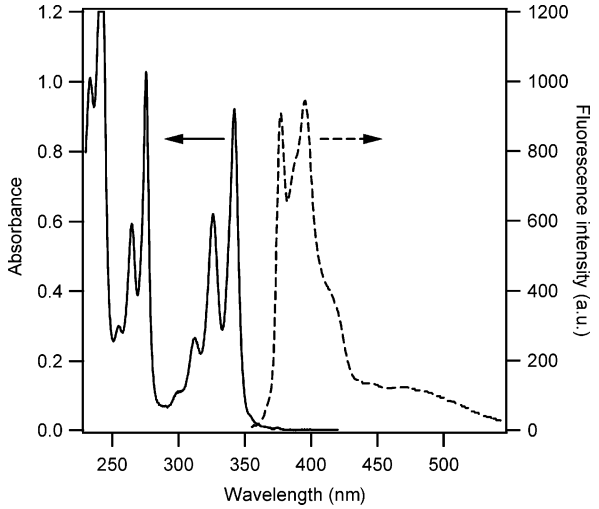

Figure 3. Absorption spectrum (solid) and fluorescence spectrum (dashed) of AcSP18Fc in ethanol.

To be exactly described, eq 8 should be corrected by the difference between work functions of the gold and the reference electrode, but the difference was omitted for simplicity here. The ϕ_{ref} value is 0 V from the definition in this study and E_{pzc} is taken from the literature (+0.33 V).[34] Finally, solving eqs 2−7 with the parameters described above, the electrostatic potentials, ϕ_2, ϕ_3, ϕ_4, and ϕ_5, as well as the charge densities at the metal surface (σ_1) and in the aqueous phase (σ_6) can be obtained.

Results and Discussion

Prior to self-assembling on gold, the conformation of the peptides in ethanol was studied by circular dichroism (CD) spectroscopy. In the CD spectra, all the peptides showed a double-minimum pattern at 208 and 220 nm, which is characteristic of α-helical conformation (Figure 2). The helix contents were 48%, 56%, 58%, and 39% for SS18Fc, Fc18SS, AcS18Fc, and AcSP18Fc, respectively. The low helix content of AcSP18Fc is probably due to the steric hindrance between the bulky pyrenyl groups and the adjacent methyl groups of the Ala or Aib residues. To investigate the interaction between the two pyrenyl groups in AcSP18Fc, absorption and fluorescence spectra in ethanol were measured (Figure 3). The absorption spectra showed the characteristic monomeric absorption of a pyrenyl group, indicating no electronic interaction between the two

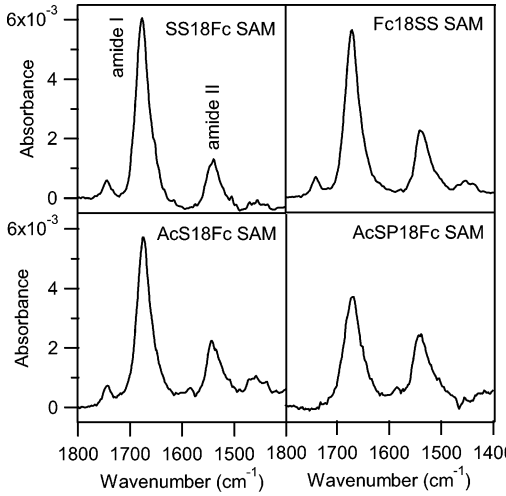

Figure 4. FTIR spectra of the helical peptide SAMs on gold.

TABLE 1: Surface Coverages of the Helical Peptide SAMs Obtained by Integration of the Oxidative Peak in the Cyclic Voltammogram, and the Theoretical Surface Coverages Assuming Hexagonal Close Packing of Helical Peptides (diameter was taken to be 1.2 nm) with the Tilt Angles Obtained by Infrared Spectroscopy

	surface coverage (mol/cm^2)	tilt angle (deg)	theoretical surface coverage (mol/cm^2)
SS18Fc SAM	9.6×10^{-11}	32	11×10^{-11}
Fc18SS SAM	11×10^{-11}	41	10×10^{-11}
AcS18Fc SAM	7.7×10^{-11}	38	10×10^{-11}
AcSP18Fc SAM	12×10^{-11}	48	8.9×10^{-11}

pyrenyl groups in the ground state. In the fluorescence spectrum, monomer emission is dominant and excimer emission is hardly observed, showing that there is no strong interaction in the excited-state either. These observations agree well with the CD observation showing that the AcSP18Fc molecule takes an α-helical conformation, in which the two pyrenyl groups are located at the opposite sides of the helix because they are separated by eight residues.

A gold substrate was immersed in an ethanol solution of each helical peptide to prepare the SAM-modified substrate. The molecular orientation of the peptide SAMs was investigated by Fourier transform infrared reflection-absorption spectroscopy (FTIR-RAS). The obtained FTIR-RAS spectra are shown in Figure 4. Amide I and amide II bands appeared around 1675 and 1545 cm^{-1}, respectively, indicating an α-helix standing vertically on the substrate surface.[22] Calculation based on the amide I/amide II absorbance ratios gave the tilt angles of the helix axis from the surface normal: 32°, 41°, 38°, and 48° for the SS18Fc, Fc18SS, AcS18Fc, and AcSP18Fc SAM, respectively (Table 1). The tilt angle in the Fc18SS SAM is larger than that in the SS18Fc. In the monolayer in which peptides are immobilized at the C-terminal, the part connecting the peptide to gold is highly negative due to the negatively charged peptide C-terminal and the negatively charged sulfur atom in a gold−sulfur linkage. This should cause lateral intermolecular electrostatic repulsion between the peptides to interrupt their good packing, leading to a large tilt angle of the peptides. A similar tendency has been observed in the other peptide monolayers immobilized at the C-terminal.[7,17,35] It was also found that the AcSP18Fc SAM has the largest tilt angle of them all. CD spectroscopy showed that the helix content of AcSP18Fc is the lowest. Further, the bulky pyrenyl groups are likely to hinder good packing of the peptides. These two factors seem to be responsible for the poorer packing and larger tilt angle of the AcSP18Fc molecules.

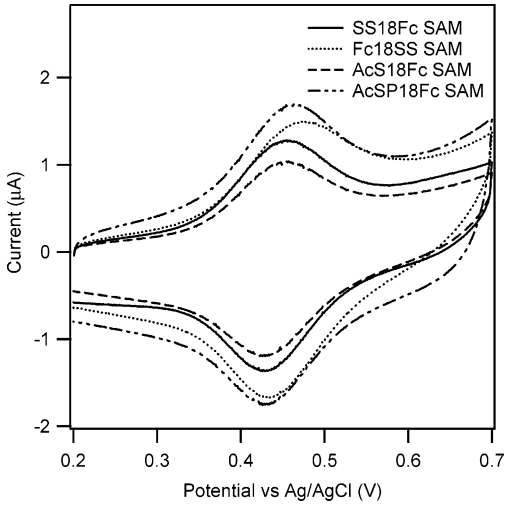

Figure 5. Cyclic voltammograms of the helical peptide SAMs in a 1 M $HClO_4$ aqueous solution at a sweep rate of 10 mV/s.

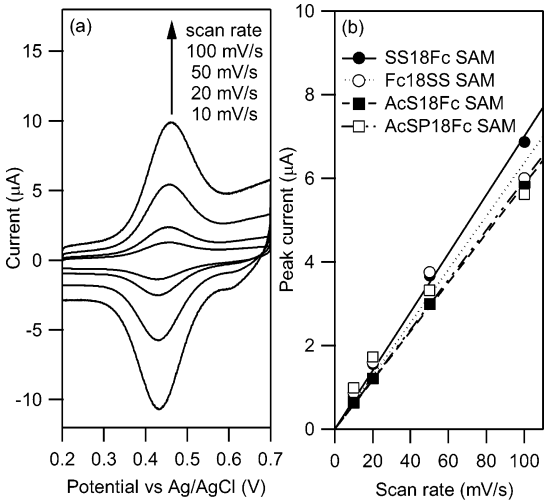

Figure 6. (a) Cyclic voltammograms of the SS18Fc SAMs in a 1 M $HClO_4$ aqueous solution at various sweep rates. (b) Dependence of the oxidative peak currents on scan rates in the helical peptide SAMs.

These SAMs were then subjected to cyclic voltammetry in a 1 M $HClO_4$ aqueous solution to investigate the electron transfer between the ferrocene moiety and gold through the peptide monolayers. Figure 5 shows the cyclic voltammograms of the peptide SAMs recorded at a scan rate of 10 mV/s. The reversible redox peaks of the ferrocene moiety were observed in all cases. The standard redox potentials were found to be independent of the dipole directions or the linker difference, nearly the same in all cases (ca. 0.45 V). This observation will be discussed in a later section. The oxidative peak current, which was obtained by subtraction of a background current from the oxidative peak current, showed a linear relationship with the scan rates (Figure 6). This result confirms that the observed redox peaks arise not from some diffusing species in the aqueous phase, but from the surface-bound ferrocene moiety. The diffusion of the ferrocene moiety of the peptides to the gold surface with the help of the bending motion of the peptide chain is also excluded, because helical peptides have a rigid cylindrical structure and the peptide monolayers were found to be well-packed as follows.

The surface coverages of the SAMs were calculated by integrating the oxidative peak after subtraction of the background current (Figure 5). The calculated surface coverages are sum-

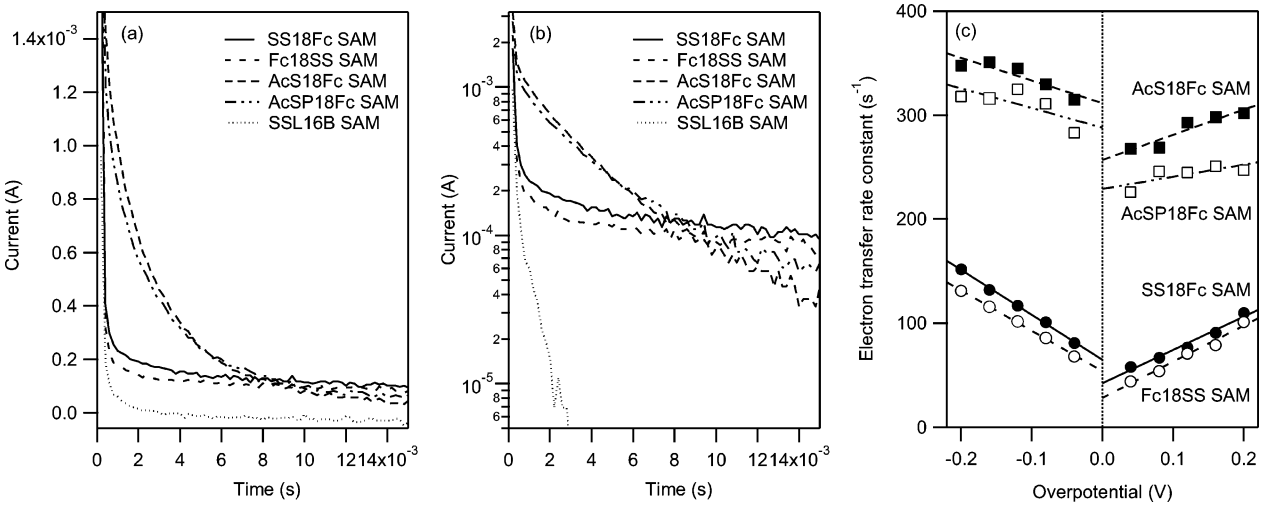

Figure 7. Results in chronoamperometry of the SAMs: (a) $i-t$ curves of the helical peptide SAMs at an overpotential of 0.04 V, (b) its semilog plots, and (c) dependence of electron-transfer rate constants on overpotentials in the electron transfer between the ferrocene moiety and gold in the helical peptide SAMs.

marized in Table 1. The coverages roughly agree with the theoretical values assuming close packing of the helical peptides with the tilt angle obtained from the infrared spectroscopy. The theoretical surface coverage of the AcSP18Fc SAM was slightly smaller than that obtained from the cyclic voltammogram. The tilt angle of the AcSP18Fc SAM, which was used for the theoretical surface coverage, might be estimated as larger than that of the actual SAM, because of some nonspecific adhesion of the peptide molecules onto the peptide monolayer.

The distances between the ferrocene moiety and gold along the molecule can be roughly estimated to be 43 Å for the SS18Fc and Fc18SS SAMs, and 41 Å for the AcS18Fc and AcSP18Fc SAMs, respectively. These distances were calculated by assuming a 1.5 Å length of one residue in an α-helix, a 1.25 Å length of one single bond in the methylene chains, and a 3.0 Å length of the phenylene chain. The cyclic voltammetry clearly indicates that long-range electron transfer over 40 Å along the molecule actually occurs. It should be noted that such long-range electron transfer hardly occurs in the conventional alkanethiol SAMs.[36]

For quantitative discussion, chronoamperometry was carried out to determine the electron-transfer rate constants for the peptide SAMs. The representative $i-t$ curves, which were recorded at an overpotential (the difference between the applied potential and the standard redox potential of the ferrocene moiety) of +0.04 V, are shown in Figure 7a in normal plots and Figure 7b in semilog plots. In interfacial electron-transfer reactions between the surface-bound redox group and metal, the current i decays exponentially with time following the equation, $i = i_0 \exp(-k_{et}t)$, where i_0, k_{et}, and t represent the initial current at $t = 0$, electron-transfer rate constant, and time, respectively.[37] The control SAM of SSL16B without a ferrocene moiety (α-helical hexadecapeptide of alternating sequence of L-leucine and α-aminoisobutyric acid with a disulfide group at the N-terminal) only showed a capacitive response in the time region of 0−2 μs (Figure 7a). On the other hand, all the SAMs with a ferrocene moiety showed an electron-transfer response (linear slopes in Figure 7b after ca. 2 μs) following the capacitive response. Therefore, the $i-t$ curves in the time region between 2 and 9 μs were analyzed by single-exponential fitting to determine the electron-transfer rate constants. Figure 7c summarizes the electron-transfer rates for the ferrocene oxidation at various positive overpotentials and those for the ferricinium reduction at various negative overpotentials. The dependence of the rate constants on applied potentials was found to be very weak compared to the cases of other SAMs composed of alkanethiols or other sulfur-terminated compounds.[23,37]

The standard rate constants for electron transfer (the rate constants at the standard redox potential) were determined by extrapolation of the data in Figure 7c to an overpotential of 0 V. For the electron transfer from the ferrocene moiety to gold, the obtained standard rate constants were 42, 28, 257, and 229 s^{-1} for the SS18Fc, Fc18SS, AcS18Fc, and AcSP18SS SAMs, respectively. On the other hand, for the back electron transfer from gold to the ferricinium, the rates were 65, 54, 312, and 288 s^{-1} for the SS18Fc, Fc18SS, AcS18Fc, and AcSP18SS SAMs, respectively.

Separately from these experiments, the mixed SAMs of SS18Fc and SSL16B with ratios of 1/3, 1/1, and 3/1 were also investigated (data not shown) to examine the contribution of intermolecular electron transfer to the total electron transfer. There was no significant difference observed for those mixed SAMs from the pure SS18Fc SAM, indicating that the electron transfer between the ferrocene moiety and gold mainly occurs through just a single molecule but does not include an intermolecular path. It is therefore considered that the difference in the surface coverages does not significantly affect the electron-transfer rates.

The theoretical values of standard electron-transfer rate constants assuming a superexchange mechanism were calculated on the basis of exponential decay constants with intervening atom number or length (tunneling constants). The standard rate constant k_{et} is expressed in the form of eq 10.

$$k_{et} = k_{et}^{0} \exp(-\beta_A n_A - \beta_B n_B - \beta_C' d_C - \beta_D' d_D) \quad (10)$$

k_{et}^{0}, β_A, and β_B represent respectively the preexponential factor, which is the electron-transfer rate between a free ferrocene in solution and electrode at the closest contact, and the tunneling constants per atom number for the methylene chain and the amide group not involved in the peptide chain, and they are taken to be 3×10^8 s^{-1}, 1.2, and 0.5, respectively, according to the literature.[23] β_C' and β_D' are the tunneling constants per length for a phenylene chain and a helical peptide chain, and they were reported to be 0.36[9] and 0.66 $Å^{-1}$,[4] respectively. In counting the number of atoms connecting the ferrocene moiety and gold, the sulfur atom and the amide group involved in the ferrocene moiety were omitted since the total length of the

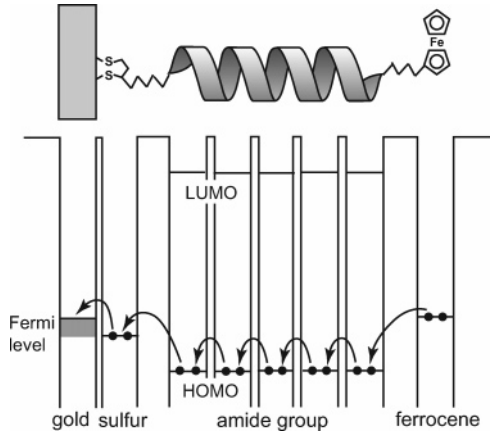

Figure 8. Energy diagram for the long-range electron transfer from the ferrocene moiety to gold through the helical peptide by a hopping mechanism with the amide groups as hopping sites.

Au−S and N−CO−C bonds is about the same as the distance between a free ferrocene in solution and electrode at the closest contact as described in the literature.[23] Therefore, the atom numbers involved in the methylene chain and amide group, n_A and n_B, are taken to be 7 and 2 for SS18Fc and Fc18SS, and 2 and 2 for AcS18Fc and AcSP18Fc, respectively. The length of the phenylene chain d_C in AcS18Fc and AcSP18Fc was assumed to be 3.0 Å. The chain length of helical peptide d_D was taken to be 27 Å assuming 1.5 Å as the length of one residue in a helical peptide. Finally, the standard rate constants k_{et} were calculated to be 0.0005 s^{-1} for the SS18Fc and Fc18SS SAMs, and 0.06 s^{-1} for the AcS18Fc and AcSP18Fc SAMs.

Notably, the experimental values of the standard rate constants (42, 28, 257, and 229 s^{-1} for the SS18Fc, Fc18SS, AcS18Fc, and AcSP18SS SAMs in the cases of electron transfer from ferrocene moiety to gold) are significantly larger than the theoretical rate constants under the assumption of a superexchange mechanism (0.0005 s^{-1} for the SS18Fc and Fc18SS SAMs, and 0.06 s^{-1} for the AcS18Fc and AcSP18Fc SAMs). It is thus a hopping mechanism that is primarily operative in the long-range electron transfer in the present systems rather than a superexchange mechanism. Furthermore, very weak dependence of the rate constants on applied potentials compared to the normal electron tunneling cases also supports that a hopping mechanism is dominant in the present systems. This point will be further discussed later. The results mentioned above agree well with the previous results.[17] The plausible hopping sites are the amide groups in the helical peptides, because the amide groups are regularly arranged and close to each other and, in fact, strong electronic interaction between them has been reported.[38]

Figure 8 shows the simple energy diagram for the electron transfer from the ferrocene moiety to gold. In the diagram, the electrostatic potential changes caused by the interfaces and the dipole moment, which will be discussed in a later section, are omitted for simplicity. Here we label the occupied orbitals localized on the ferrocene moiety and the sulfur atom as "ferrocene HOMO" and "S HOMO", and similarly label the unoccupied and occupied orbital localized on the amide group as "amide LUMO" and "amide HOMO", respectively. These orbital energies were calculated by ab initio calculation with Gaussian 03 program. The carrier is considered to be a hole because the amide LUMO (−1.2 eV) is so high that the electron injection from the ferrocene moiety (ferrocene HOMO energy is −5.1 eV) to the amide group is unlikely to occur. Therefore, the overall electron-transfer reaction from the ferrocene moiety to gold is composed of three processes: electron transfer to gold from the nearest amide group, electron hopping among the amide groups, and electron transfer from the ferrocene moiety to the nearest amide group. The first process can further be divided into two processes, electron transfer from the sulfur atom to gold and that from the amide group to the sulfur atom, because the S HOMO level (−5.5 eV) is located between the gold Fermi level (−5.1 eV) and the amide HOMO level (−6.5 eV). Although these levels should shift in the monolayer on gold by the effects of the metal surface and electrostatic potential profile, the qualitative relationship among them is considered not to be changed.

From comparison of the SS18Fc SAM with the Fc18SS SAM, where dipole moment directions are opposite, the dipole moment did not affect significantly the rate constants (42 and 28 s^{-1} respectively for the SS18Fc and Fc18SS SAMs). On the other hand, changing the linker from a methylene chain to a more conductive phenylene chain remarkably accelerated electron transfer: the rate constant in the SS18Fc SAM was 42 s^{-1}, whereas that in the AcS18Fc SAM was 257 s^{-1}. From these results, the local electron transfer between gold and the molecular terminal of the helical peptides should be the rate-determining step, while the electron hopping process via the amide groups is relatively fast among all the electron-transfer processes. Considering that the chemically adsorbed sulfur atom on gold strongly couples with the gold surface, the electron transfer from the sulfur atom to gold should be faster than that from the amide group to the sulfur atom through the linker. The latter process is thus considered to be the rate-determining step. The phenylene linker is considered to promote the electron transfer from the amide group to the sulfur atom due to its higher electron conductivity due to the π electrons compared to the methylene chain.

Meanwhile, the electron-transfer rate in the AcSP18Fc SAM with two pyrenyl groups was in the same order as that in the AcS18Fc SAM without pyrenyl groups, indicating that introduction of two pyrenyl groups into the side chains of the helical peptides does not accelerate the electron transfer. In the present systems, the rate-determining step is not the electron hopping among the amide groups but the electron transfer localized near gold. Thus, even if the pyrenyl groups could facilitate electron transfer remarkably through the peptide part, the overall reaction apparently would be unchanged. Further, additional hopping processes between the pyrenyl groups, the ferrocene moiety and the pyrenyl group, and gold and the pyrenyl group are not likely to occur because the distances are too long for efficient electron hopping.

To validate the several features found in the present work, electrostatic potential profiles though the monolayer are calculated by using a simple metal/monolayer/solution model on the basis of Gauss' law. The monolayer is composed of four layers of different dielectric constants: gold surface−sulfur atom, methylene linker, helical peptide, and the connector between the peptide and the ferrocene moiety. The potential profiles in the SS18Fc and Fc18SS SAMs at various applied potentials including the redox potential of the ferrocene moiety (0.45 V) are shown in Figure 9. In each case, the electrostatic potential at the ferrocene moiety coincides well with the solution potential (0.33 V) because of the high concentration of electrolyte in solution (1 M $HClO_4$). Regardless of the superexchange mechanism or the hopping mechanism, the standard potential represents that the Fermi level of gold equals the redox potential of the ferrocene moiety in solution. Therefore, the results of the calculation above are in good agreement with the experi-

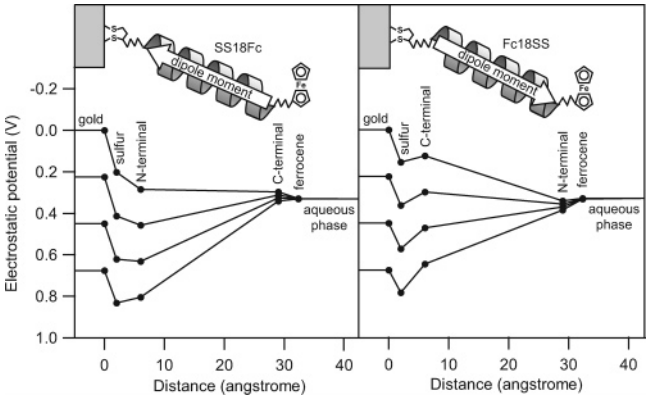

Figure 9. Calculated electrostatic potential profiles in the SS18Fc and Fc18SS SAMs on various applied potentials of gold including the standard redox potential of the ferrocene moiety (0.45 V).

mental observation that redox potentials were nearly the same between the SS18Fc and Fc18SS SAMs irrespective of their dipole directions.

As shown in Figure 9, upon applying potential on gold, most of the applied potential drops within the helical peptide layer, while the potential difference in the methylene linker layer is kept small. This explains the observed weak dependence of the rate constants on the applied potentials, because the electron transfer through the linker is considered to be the rate-determining step. The forward electron transfer from the ferrocene moiety to gold in the Fc18SS SAM should be faster than that in the SS18Fc SAM because the former shows the negative slope in the potential profile to accelerate the forward electron transfer. However, the experimental value in the Fc18SS SAM was slightly smaller than that in SS18Fc SAM. The linker of Fc18SS between the sulfur atom and the peptide terminal is longer with one methylene group than that of SS18Fc, although the total number of atoms between the sulfur atom and the ferrocene moiety of Fc18SS and SS18Fc were designed to be the same. This factor should counterbalance the effect of the potential difference between the amide group at the terminal and the sulfur atom in the electron transfer across this region of the Fc18SS SAM, incidentally leading to a comparable rate to the SS18Fc SAM.

The rate constants for the ferricinium reduction were slightly larger than those for the ferrocene oxidation (Figure 7c). The rates in forward and backward electron transfer are generally the same in the molecular system where a superexchange mechanism is applicable. However, such similarity is unusual in the case of a hopping mechanism. That is, from the viewpoint of the driving force, the rate-determining step for the forward electron transfer from ferrocene to gold should be the electron transfer from the amide group at the terminal to the sulfur as described before. On the other hand, the rate-determining step for the backward electron transfer from gold to the ferricinium appears to be the electron transfer from the amide group at the opposite terminal to the ferricinium (electron flow opposite to that in Figure 8). In the present case, however, the rate-determining step is always the electron transfer between the amide group at the terminal and the sulfur. It is speculated that the amide group, which is connected directly to the ferrocene moiety, may electronically couple strongly to the amide group at the peptide terminal to make the electron transfer across the peptide chain and the ferrocene moiety fast. We need to clarify the electron-transfer properties at the interfaces more precisely in future work.

Conclusion

Four different kinds of helical octadecapeptides carrying a ferrocene moiety at the terminal were respectively self-assembled on gold, and effects of the dipole moment of the helical peptide, the linkers connecting the peptide to gold, and the chromophores introduced in the side chains on the long-range electron transfer through the monolayers were investigated. Cyclic voltammetry and chronoamperometry revealed that long-range electron transfer over 40 Å actually occurred according to a hopping mechanism, using the amide groups in the helical peptide as hopping sites. The dipole moment affected neither the redox potential of the ferrocene moiety nor the electron-transfer rates. On the other hand, the substitution of a methylene chain with a phenylene linker led to the remarkable acceleration of electron transfer, showing that the electron transfer through the linker determines the overall electron-transfer rate. Introduction of chromophores into the side chains did not affect the electron transfer significantly, probably due to their unfavorable location for the acceleration of the rate-determining step or additional hopping process with the chromophores as hopping sites. Calculation of electrostatic potential profiles across the monolayers could consistently explain several features observed in the present systems. For future work, the linker between the peptide and gold will be optimized to accelerate the electron transfer, simply by shortening a linker or by introduction of a chromophore near the gold surface. These challenges will enable more efficient long-range electron transfer, and will also bring out a rectifying property based on the dipole moment of the helical peptides. The actual redox potentials, not mere frontier orbital energies used in this study, of the amide group and the sulfur atom in the monolayer should be estimated by ab intio calculation for further quantitative discussion on the electron-transfer kinetics. Distance dependence of the electron transfer should also be examined to gain more information on the mechanism. As long as a hopping mechanism is operative in electron transfer across the helical peptides, elongation of the peptide chains will not reduce the electron-transfer rate severely. 32 mer and 48 mer helical peptides are synthetically available and we predict, on the basis of the results obtained in the present work, they will show unprecedented, extraordinarily long-range electron transfer over 80 and 120 Å.

Acknowledgment. This work is partly supported by Grant-in-Aids for Young Scientists B (16750098) and for Scientific Research B (15350068), and 21st century COE program, COE for a United Approach to New Materials Science, all from the Ministry of Education, Culture, Sports, Science, and Technology, Japan.

References and Notes

(1) Page, C. C.; Moser, C. C.; Chen, X. X.; Dutton, P. L. *Nature* **1999**, *402*, 47−52.
(2) Wasielewski, M. R. *Chem. Rev.* **1992**, *92*, 435−461.
(3) Beratan, D. N.; Onuchic, J. N.; Winkler, J. R.; Gray, H. B. *Science* **1992**, *258*, 1740−1741.
(4) Sisido, M.; Hoshino, S.; Kusano, H.; Kuragaki, M.; Makino, M.; Sasaki, H.; Smith, T. A.; Ghiggino, K. P. *J. Phys. Chem. B* **2001**, *105*, 10407−10415.
(5) Hol, W. G. J. *Prog. Biophys. Mol. Biol.* **1985**, *45*, 149−195.
(6) Fox, M. A.; Galoppini, E. *J. Am. Chem. Soc.* **1997**, *119*, 5278−5279.
(7) Morita, T.; Kimura, S.; Kobayashi, S.; Imanishi, Y. *J. Am Chem. Soc.* **2000**, *122*, 2850−2859.
(8) Yasutomi, S.; Morita, T.; Imanishi, Y.; Kimura, S. *Science* **2004**, *304*, 1944−1947.
(9) Creager, S.; Yu, C. J.; Bamdad, C.; O'Connor, S.; MacLean, T.; Lam, E.; Chong, Y.; Olsen, G. T.; Luo, J.; Gozin, M.; Kayyem, J. F. *J. Am. Chem. Soc.* **1999**, *121*, 1059−1064.

(10) Fan, F. R. F.; Yao, Y. X.; Cai, L. T.; Cheng, L.; Tour, J. M.; Bard, A. J. *J. Am. Chem. Soc.* **2004**, *126*, 4035−4042.
(11) Davis, W. B.; Svec, W. A.; Ratner, M. A.; Wasielewski, M. R. *Nature* **1998**, *396*, 60−63.
(12) Sikes, H. D.; Smalley, J. F.; Dudek, S. P.; Cook, A. R.; Newton, M. D.; Chidsey, C. E. D.; Feldberg, S. W. *Science* **2001**, *291*, 1519−1523.
(13) Petrov, E. G.; Shevchenko, Ye. V.; Teslenko, V. I.; May, V. *J. Chem. Phys.* **2001**, *115*, 7107−7122.
(14) Petrov, E. G.; May, V.; Haengi, P. *Chem. Phys.* **2002**, *281*, 211−224.
(15) Bixon, M.; Jortner, J. *J. Phys. Chem. B* **2000**, *104*, 3906−3913.
(16) Berlin, Y. A.; Burin, A. L.; Ratner, M. *J. Am. Chem. Soc.* **2001**, *123*, 260−268.
(17) Morita, T.; Kimura, S. *J. Am. Chem. Soc.* **2003**, *125*, 8732−8733.
(18) Otoda, K.; Kimura, S.; Imanishi, Y. *Biochim. Biophys. Acta* **1993**, *1145*, 33−41.
(19) Chen, Y. H.; Yang, J. T.; Martinez, H. M. *Biochemistry* **1972**, *11*, 4120−4131.
(20) Gremlich, H. U.; Frigeli, U. P.; Schwyzer, R. *Biochemistry* **1983**, *22*, 4257−4264.
(21) Tsuboi, M. *J. Polym. Sci.* **1962**, *59*, 139.
(22) Kennedy, D. F.; Chrisma, M.; Chapman, T. D. *Biochemistry* **1991**, *30*, 6541−6548.
(23) Sek, S.; Palys, B.; Bilewicz, R. *J. Phys. Chem. B* **2002**, *106*, 5907−5914.
(24) CAChe Worksystem Pro Version 6.1.1; Fujitsu Limited: Tokyo, Japan, 2003.
(25) Frisch, M. J.; Trucks, G. W.; Schlegel, H. B.; Scuseria, G. E.; Robb, M. A.; Cheeseman, J. R.; Montgomery, J. A., Jr.; Vreven, T.; Kudin, K. N.; Burant, J. C.; Millam, J. M.; Iyengar, S. S.; Tomasi, J.; Barone, V.; Mennucci, B.; Cossi, M.; Scalmani, G.; Rega, N.; Petersson, G. A.; Nakatsuji, H.; Hada, M.; Ehara, M.; Toyota, K.; Fukuda, R.; Hasegawa, J.; Ishida, M.; Nakajima, T.; Honda, Y.; Kitao, O.; Nakai, H.; Klene, M.; Li, X.; Knox, J. E.; Hratchian, H. P.; Cross, J. B.; Adamo, C.; Jaramillo, J.; Gomperts, R.; Stratmann, R. E.; Yazyev, O.; Austin, A. J.; Cammi, R.; Pomelli, C.; Ochterski, J. W.; Ayala, P. Y.; Morokuma, K.; Voth, G. A.; Salvador, P.; Dannenberg, J. J.; Zakrzewski, V. G.; Dapprich, S.; Daniels, A. D.; Strain, M. C.; Farkas, O.; Malick, D. K.; Rabuck, A. D.; Raghavachari, K.; Foresman, J. B.; Ortiz, J. V.; Cui, Q.; Baboul, A. G.; Clifford, S.; Cioslowski, J.; Stefanov, B. B.; Liu, G.; Liashenko, A.; Piskorz, P.; Komaromi, I.; Martin, R. L.; Fox, D. J.; Keith, T.; Al-Laham, M. A.; Peng, C. Y.; Nanayakkara, A.; Challacombe, M.; Gill, P. M. W.; Johnson, B.; Chen, W.; Wong, M. W.; Gonzalez, C.; Pople, J. A. *Gaussian 03*; Gaussian, Inc.: Wallingford, CT, 2004.
(26) Smith, C. P.; White, H. S. *Anal. Chem.* **1992**, *64*, 2398−2405.
(27) Lecomte, S.; Hildebrandt, P.; Soulimane, T. *J. Phys. Chem. B* **1999**, *103*, 10053−10064.
(28) Evans, S. D.; Ulman, A. *Chem. Phys. Lett.* **1990**, *170*, 462−466.
(29) Jaworek, T.; Neher, D.; Wegner, G.; Wieringa, R. H.; Schouten, A. J. *Science* **1998**, *279*, 57−60.
(30) Narioka, S.; Ishii, H.; Yoshimura, S.; Sei, M.; Ouchi, Y.; Seki, K. *Appl. Phys. Lett.* **1995**, *67*, 1899−1901.
(31) Ito, E.; Oji, H.; Ishii H.; Oichi, K.; Ouchi, Y.; Seki, K. *Chem. Phys. Lett.* **1998**, *287*, 137−142.
(32) Alloway, D. M.; Hofmann, M.; Smith, D. L.; Gruhn, N. E.; Graham, A. L.; Colorado, R.; Wysochi, V. H.; Lee, T. R.; Lee, P. A.; Armstrong, N. R. *J. Phys. Chem. B* **2003**, *107*, 11690−11699.
(33) Imanishi, Y.; Miura, Y.; Iwamoto, M.; Kimura, S.; Umemura, J. *Proc. Jpn. Acad., Ser. B* **1999**, *75*, 287−290.
(34) Hamm, U. W.; Kramer, D.; Zhai, R. S.; Kolb, D. M. *J. Electroanal. Chem.* **1996**, *414*, 85−89.
(35) Miura, Y.; Kimura, S.; Kobayashi, S.; Imanishi, Y.; Umemura, J. *Biopolymers* **2000**, *55*, 391−398.
(36) Chidsey, C. E. D.; Bertozzi, C. R.; Putvinski, T. M.; Mujsce, A. M. *J. Am. Chem. Soc.* **1990**, *112*, 4301−4306.
(37) Flinklea, H. O.; Hanshew, D. D. *J. Am. Chem. Soc.* **1992**, *114*, 3173−3181.
(38) Shin, Y. K.; Newton, M. D.; Isied, S. S. *J. Am. Chem. Soc.* **2003**, *125*, 3722−3732.